Geoderma 433 (2023) 116464

Contents lists available at ScienceDirect

Geoderma

journal homepage: www.elsevier.com/locate/geoderma

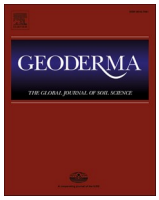

Structure turnover times of grassland soils under different moisture regimes

Frederic Leuther [a,c,*,1], Robert Mikutta [b,2], Maximilian Wolff [b,3], Klaus Kaiser [b,4], Steffen Schlüter [a,5]

[a] Department of Soil System Science, Helmholtz-Centre for Environmental Research – UFZ GmbH, Halle (Saale), Germany
[b] Soil Science and Soil Protection, Martin Luther University Halle-Wittenberg, Halle (Saale), Germany
[c] Department of Soil and Environment, Swedish University of Agricultural Sciences, Uppsala, Sweden

ARTICLE INFO

Handling Editor: Yvan Capowiez

Keywords:
Soil structure
Bioturbation
Carbon turnover
Physical protection
Soil moisture

ABSTRACT

Soil structure is a dynamic property of soils, which refers to temporal changes in the spatial arrangement of pores, organic matter, and minerals. Its turnover, i.e. the irreversible redistribution of soil constituents, determines essential soil functions including carbon storage. Structure turnover times and its response to biotic versus abiotic drivers have never been quantified directly under natural conditions. We used a novel combination of structure labelling with inert garnet particles and X-ray Computed Tomography to determine structure turnover times of two grassland topsoils with either access or exclusion of roots and fauna > 30 μm. Both, abiotic and biotic factors developed soil structure at a site-specific rate towards a dynamic equilibrium, at which bulk properties remain constant because creation and destruction of structural properties are in balance. Its turnover, however, was mainly determined by macrofaunal activity which varied with environmental conditions. Under dry conditions less favorable for bioturbation, the extrapolated structure turnover time was 33 ± 3 years, while being 16 ± 1 years under moist conditions. Previous studies on organic matter turnover determined in the vicinity of the experimental site showed similar turnover times for particulate organic matter. The similar turnover times suggest that the accessibility of particulate organic matter to decomposers is closely linked to structure turnover, thus highlighting the intimate nexus between structure evolution and carbon persistence in soil.

1. Introduction

Soil structure, the three-dimensional arrangement of solid soil constituents and pores, results from the complex interplay of various physical, chemical, and biological processes (Vogel et al., 2022; Young and Crawford, 2004). These processes continuously alter soil architecture with impacts on various soil functions, such as carbon and water storage and nutrient recycling (Rabot et al., 2018). One key mechanism regulating soil organic matter turnover is physical protection by limited accessibility for microbial decomposers (Lehmann and Kleber, 2015). Incubation experiments have shown that oxygen availability and the coexistence of different microbial communities in different pore sizes influence the mineralization of organic matter (Nunan et al., 2017; Ruamps et al., 2011; Strong et al., 2004): Macropores with a diameter >120 μm are typically drained under field conditions and biological activity is therefore limited through water scarcity; small micro- and nanopores (diameter < 1 μm) limit bacterial growth by their size and by water logging (Keiluweit et al., 2016; Keiluweit et al., 2017). The continuous rearrangement of soil structure and thus, the change in spatial accessibility of organic matter described by the distance to pores more favourable for microbial activity is a valuable indicator for physical protection (Ortega-Ramírez et al., 2023; Schlüter et al., 2022). However, approaches to link the long-term persistence of soil carbon to soil structure turnover in ecosystem models are still in their infancy (Meurer et al., 2020b) essentially because 1) proper estimates of soil structure turnover rates are lacking and 2) formalisms how to quantitatively link carbon turnover to physical protection in intact pore space need to be improved. In this paper, we demonstrate how the first

* Corresponding author at: Department of Soil and Environment, Swedish University of Agricultural Sciences, Uppsala, Sweden.
E-mail address: frederic.leuther@uni-bayreuth.de (F. Leuther).
[1] ORCID: 0000-0001-6955-7892.
[2] ORCID: 0000-0002-7186-6528.
[3] ORCID: 0000-0003-0226-7246.
[4] ORCID: 0000-0001-7376-443X.
[5] ORCID: 0000-0002-3140-9058.

https://doi.org/10.1016/j.geoderma.2023.116464
Received 9 January 2023; Received in revised form 29 March 2023; Accepted 2 April 2023
Available online 6 April 2023
0016-7061/© 2023 The Authors. Published by Elsevier B.V. This is an open access article under the CC BY license (http://creativecommons.org/licenses/by/4.0/).

challenge can be overcome and provide experimental field data to address the second challenge.

Biological processes like root growth (Hinsinger et al., 2009), organic matter decomposition (Young and Crawford, 2004), and faunal activities (Bottinelli et al., 2015) shape soil structure by bioturbation, creation of biopores, and exudation of binding agents. Soil mesofauna (width 0.1–2 mm) and macrofauna (width 2–200 mm) mix mineral and organic particles in their guts (Coleman et al., 2017) and produce casts of different sizes and densities (Briones, 2014; Michel et al., 2022). Earthworms transport material from the soil surface to deeper soil and produce burrow walls with compacted zones that can contain increased amounts of stabilized organic carbon (Capowiez et al., 2011; Don et al., 2008). Social insects, such as ants, form networks of pores in topsoils while creating nests and galleries by displacing soil constituents (Bottinelli et al., 2015). Also, soil fauna regulates microbial populations, which metabolize organic matter to satisfy their nutrient and energy needs (Erktan et al., 2020). In the mid-latitudes, biological processes can be limited by temperature in winter or water availability in summer, making abiotic factors such as freezing, thawing, wetting, and drying more important for soil structure change. Clay minerals, organic matter, and polyvalent cations are well known factors supporting soil structural stability. Depending on content of expandable clay minerals, the formation of desiccation cracks can strongly affect soil structure but this effect is mostly reversible upon rewetting and thus undergoes recurrent changes (Bodner et al., 2013; Cheik et al., 2021; Diel et al., 2019; Peng et al., 2007; Wang et al., 2017). Freeze-thaw cycles can fragment soil clods and increase the connectivity of pores (Leuther and Schlüter, 2021; Ma et al., 2019; Starkloff et al., 2017). There is strong evidence that structure changes evoked by cyclic abiotic processes are mostly reversible (Diel et al., 2019; Vogel et al., 2022), and therefore its potential to induce soil structure turnover as characterized by extensive, irreversible redistribution of soil constituents is limited compared to that of bioturbation (Fig. 1b).

Obtaining an integral measure of soil structure turnover in intact soil still poses a tremendous scientific obstacle. Historically, soil structure turnover has been estimated by various indirect approaches. For example, ^{13}C labelling was used to track the incorporation of organic matter into operationally defined aggregate size or density fractions (Amelung et al., 2008). This concept links the physical protection of soil organic matter to the turnover times of aggregates (Jastrow et al., 2007).

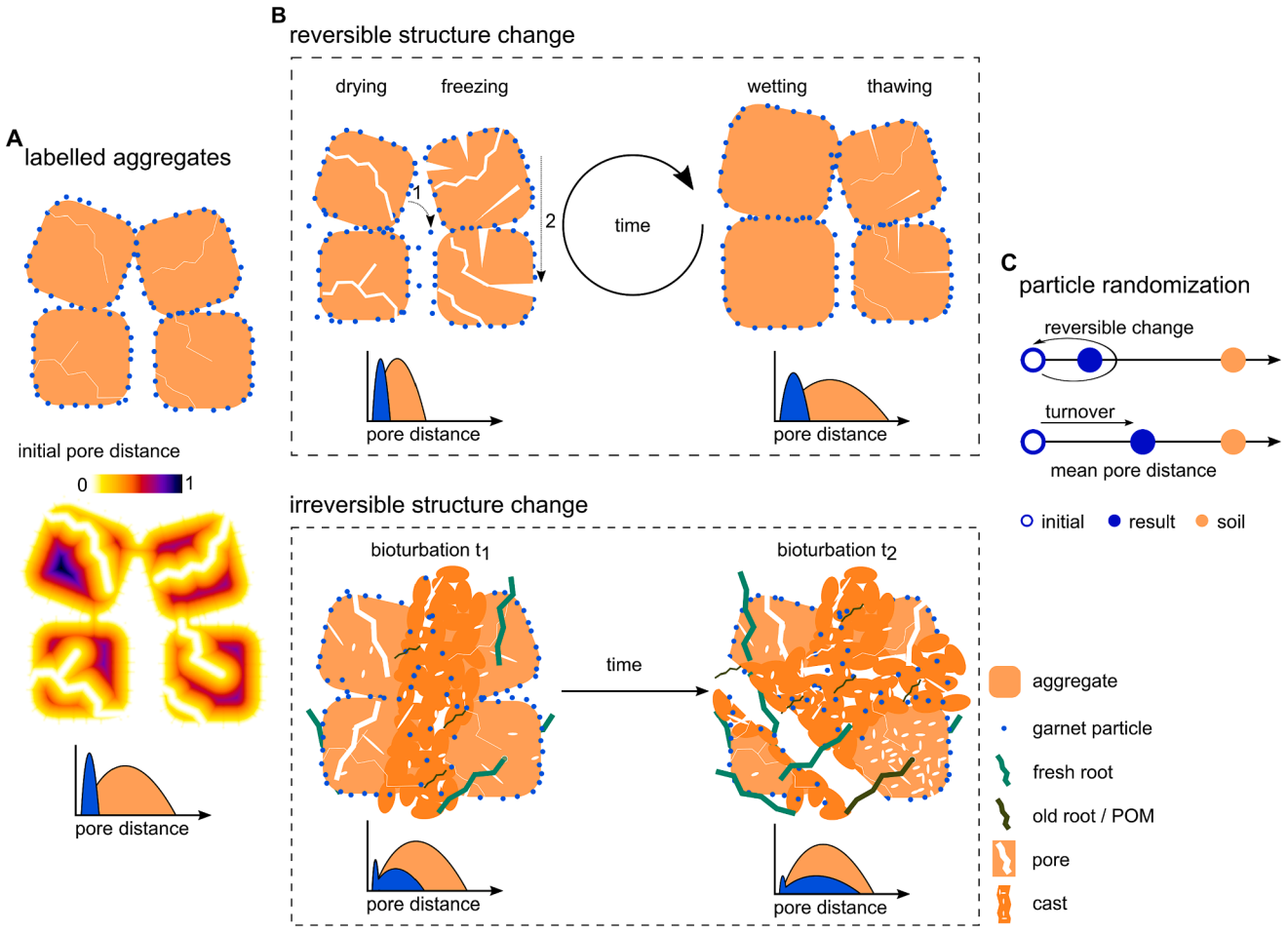

Fig. 1. Concept to measure randomization rates of soil structure turnover with garnet-labelled aggregates. A. Initial structure of aggregates labelled with garnet particles (blue), where the distance of particles to the next pore is shorter than pore distances in soil matrix. B. Drying can cause mineral shrinkage and crack formation, freezing mainly creates new pores. Both processes affect pore distances of the soil matrix but not for particles. Wetting and thawing can cause mineral swelling and mostly reverse these changes back to the initial stage. Arrow 1 indicates detachment of garnet particles from aggregate surfaces when soil is dry, arrow 2 settlement of the initial structure along recurrent freeze – thaw and wetting – drying cycles. Bioturbation irreversibly changes soil structure and the position of particles. Randomization of particles within the newly created soil structure increases with time. The amount of particles in bulk soil can decrease due to the incorporation of non-labelled soil from outside the mesocosm. C. Concept of particle randomization by non-reversible structure turnover (biotic factors) and reversible changes in soil structure (abiotic factors) based on the mean pore distance of particles and soil matrix. Structure turnover can be tracked by garnet labelling for as long as the pore distances of particles have not yet reached the average pore distance in the soil matrix. (For interpretation of the references to colour in this figure legend, the reader is referred to the web version of this article.)

However, often there is a discrepancy between the turnover of aggregates and that of carbon within aggregates (Totsche et al., 2018), which hampers straightforward conclusions on soil structure turnover. Other approaches utilize small dye-labelled ceramic tracers (Plante et al., 2002) or rare-earth oxide particles (De Gryze et al., 2006; Liu et al., 2019) in combination with modelling to derive estimates of soil structure turnover time. These approaches also rely on recovering the tracer in aggregate size fractions obtained after physically disrupting the soil, and thus, provide little information on the spatiotemporal development of soil structure. Another way of quantifying soil structure turnover involves repeated sampling at the same site to determine temporal changes of specific soil structure properties, such as pore size distribution, but long-term monitoring studies are rare (Keller et al., 2021; Lucas et al., 2019b). Using mesocosms exposed to ambient soil conditions and repeatedly scanned by X-ray Computed Tomography (X-ray μCT) at regular time intervals, average pore properties can even be tracked within the same sample (Garbout et al., 2013; Koestel and Schlüter, 2019). However, a clear distinction needs to be made between changes in average properties and soil structure turnover: As for many chemical reactions, also soil structure can be at a state of dynamic equilibrium, in which bulk properties, such as macroporosity, average pore size, and others apparently remain constant even though pores are formed and destroyed continuously. On the long term, the creation and destruction of structural features are in balance as long environmental conditions, such as climate or cover crops, do not change or no external disturbances, such as tillage, become effective. Therefore, a completely new methodological approach beyond description of average pore properties was required to quantify soil structure turnover. An approach for direct estimation of soil structure turnover has been developed based on structure labelling with inert garnet particles and X-ray μCT analysis (Schlüter and Vogel, 2016). The method enables the determination of the turnover of soil structure by tracking garnet particle randomization in soil matrix and pore spaces under field conditions (Fig. 1). Conceptually, this approach corresponds to a pool dilution experiment with stable isotopes (Murphy et al., 2003), with the pool of short distances between garnet particles and pores becoming diluted during soil structure turnover. Assuming the garnet particles reflect the redistribution of soil particles, the method allows for directly linking structure turnover to changes in potential accessibility of soil carbon for microbial decomposition.

In this study, we aimed at quantifying soil structure turnover under field conditions for several years and determining the relative contribution of different drivers covering biotic and abiotic processes. To do so, we monitored the structure of field-exposed soil mesocosms made of sieved aggregates labelled with inert garnet particles. The rate at which the location of garnet particles becomes randomized with respect to pore distances was recorded at regular time intervals for up to four years and yielded a direct estimate of soil structure turnover times. Initially, most garnet particles were located directly at pore walls with a shorter mean pore distance than the average soil matrix (Fig. 1a). The faster they became incorporated into the soil matrix, the shorter the soil structure turnover time. The turnover can be monitored for as long as the average pore distance for garnet particles has not yet reached the average pore distance within the soil matrix (Fig. 1c). Field experiments were established in topsoils (5–15 cm depth) of a Haplic Chernozem developed under dry moisture regimes and a Stagnic Luvisol formed under moist conditions, both with silty loam texture and under long-term grasslands. The environmental conditions of the soils have been shown to result in different soil faunal abundances, with higher abundance of meso- and macrofauna in Luvisol than the Chernozem topsoil (Scheunemann et al., 2010; Yin et al., 2019). Similar as for litter bags, we excluded soil fauna and root activity in half of the mesocosms using nylon gauze (30 μm mesh size) to distinguish between predominantly abiotic versus abiotic and biotic drivers of soil structure turnover. We analyzed the entire mesocosms with X-ray μCT to record soil structure development at the millimeter to centimeter scale six times at different seasons across several years. Additional subsamples were taken and measured at high spatial resolution (detectable features $>$ 30 μm) in order to assess the degree of garnet label randomization and identify structural entities formed by biological activity at the micro- to millimeter scale. The structure turnover time was compared to organic matter turnover rates previously determined on nearby sites to evaluate the importance of structure-dependent accessibility. Soil structure of undisturbed samples taken in the vicinity of the mesocosms was used as reference to capture the state of structural dynamic equilibrium under the ambient soil conditions and to evaluate the evolution of a repacked structure towards equilibrium. We hypothesized that (i) biotic and abiotic structure-forming factors modulate soil structure turnover to different extent, (ii) the extend will be dependent on the site-specific environmental conditions, and (iii) soil structure turnover times can be directly linked to organic matter turnover times.

2. Materials and methods

2.1. Study sites

Topsoil under grassland was investigated at two study sites with different climatic conditions (Table 1). The long-term field site in Bad Lauchstädt (51.3937N, 11.8786E) was located 114 m above sea level, had a mean annual temperature of 8.8 °C, and a mean annual precipitation of 484 mm. The rather continental climate at the study site was characterized by periods of low rainfall in combination with a higher sunshine duration leading to a negative climatic water balance of $<$ -150 mm during growing season (Grosse et al., 2020). The soil was a Haplic Chernozem (WRB classification), soil texture was a silty loam (110 g kg^{-1} sand, 680 g kg^{-1} silt, 210 g kg^{-1} clay), and bulk density was 1.46 g cm^{-3} in an adjacent reference profile (Altermann et al., 2005). The long-term field site in Rotthalmünster (48.3601N, 13.1921E) was located 362 m above sea level, had a mean annual temperature of 8.7 °C, and a mean annual precipitation of 886 mm (Kögel-Knabner et al., 2008). The climate was characterized as temperate and humid with a neutral climatic water balance of −50 to $<$ 50 mm during growing season (Grosse et al., 2020). The soil was a Stagnic Luvisol (WRB classification), soil texture was a silty loam (100 g kg^{-1} sand, 710 g kg^{-1} silt, 190 g kg^{-1} clay), and bulk density was 1.42 g cm^{-3}. Both soils had similar clay mineral assemblage, with contribution of individual phases in the order of illite $>$ kaolinite $>$ vermiculite. The soil slightly differed in organic carbon contents. At 5–15 cm depth, the Chernozem and the Luvisol had a total organic carbon content of 20.6 g kg^{-1} (Altermann et al., 2005) and 13.9 g kg^{-1}, respectively. The experimental sites were managed as grasslands without soil tillage for $>$60 years.

2.2. Mesocosm preparation and sampling design

For establishing the mesocosm experiments, intact grass sods were carefully removed and a pit of 450 cm length × 200 cm width × 20 cm depth was excavated. The excavated soil was air-dried and sieved to 2 to 5 mm. For each study site, 36 polycarbonate cylinders (10 cm height, 10 cm diameter, 694 cm^3) were perforated (about 100 holes) with a driller of 10 mm diameter (Fig. S1b) to serve as mesocosms under field-exposed conditions. The size of the mesocosms and holes were selected to allow for representative capturing bioturbation by macrofauna. Ends were covered with open lids that were reinforced with a coarse nylon mesh of 4 mm mesh size. Half of the 36 cylinders were additionally lined with a nylon gauze with 30 μm mesh size to exclude roots and macrofauna (Fig. S1b).

The mesocosms were filled with garnet-coated aggregates. Aggregates of 2–5-mm size were dried in an oven at 50 °C for 4 days until reaching a residual water content of 10 g kg^{-1}. The size of aggregates represents a trade-off. They are much larger than the garnet particles so that the potential for incorporation of particles in the soil matrix and occlusion from visible pores is reasonably high. At the same time, they

Table 1
Study site characteristics: soil classification (WRB), soil texture, total organic carbon content (TOC), bulk density (BD), mean annual temperature, and mean annual precipitation.

Study site	WRB	Sand [g kg^{-1}]	Silt [g kg^{-1}]	Clay [g kg^{-1}]	TOC [g kg^{-1}]	BD [g cm^{-3}]	Temperature [°C]	Precipitation [mm]
Bad Lauchsädt	Haplic Chernozem	110	680	210	20.6	1.46	8.8	484
Rotthalmünster	Stagnic Luvisol	100	710	190	13.9	1.42	8.7	886

are small enough to ensure even distribution within the mesocosms and high exposure to biotic and abiotic factors. Large root residues were removed. For each mesocosm 1 kg of soil aggregates were sprayed with 200 g of water, mixed on a tray, and covered with a lid. After 1 h of hydraulic equilibration, 160 g of the moistened aggregates were mixed with 10 g of garnet particles to cover the aggregate surface; loosely attached garnet particles were removed by gentle sieving. The garnet particles (Garnit #240, Kuhmichel Abravis GmbH, Germany), consisting of the iron-rich nesosilicate almandine with 330 g kg^{-1} Fe_2O_3, had a particle size of 45 to 100 μm. Such iron-bearing particles with high X-ray attenuation and a specific size range can be easily distinguished from the surrounding soil by X-ray CT as long as the fine sand fraction with similar characteristics is low (Schlüter and Vogel, 2016). Mesocosms for the Chernozem trial were packed with the labelled aggregates in intervals of 160 g to a bulk density of 1.35 g cm^{-3}, which is slightly lower than the topsoil bulk density of adjacent grassland. This might have created a more connected macropore network being attractive for preferential root growth. We therefore decided to slightly increase the bulk density of the Luvisol mesocosms (1.42 g cm^{-3}) representing the natural bulk density on site.

Enough mesocosms were installed to allow for five sampling times with six replicates per treatment and sampling time. Three of these replicates per treatment were sampled at every sampling date for X-ray μCT scanning of the entire mesocosm, and then re-buried. The other three mesocosms per treatment were scanned only once and then used for destructive subsampling. No systematic differences in any pore metric due to transportation and re-burring were determined between these groups of replicates. The 36 mesocosms were labelled according to the sampling date (1, 2, 3, 4, 5, and E for every sampling date), paired and randomly buried in the excavated soil pit mentioned above (Fig. S1a). The gaps between the cylinders were filled with soil, and a layer of 5 cm of soil was added on top of the samples (Fig. S1c). Similar X-ray absorption of the soil matrix of both treatments as well as the moisture conditions observed during subsampling indicated that the nylon gauze did not constrain water exchange between the mesocosms and the surrounding soils. Finally, the experimental plot was re-covered with the intact grass sods. This resulted in a final installation depth of approx. 5–15 cm. The Chernozem trial started in April 2017 and sampling occurred after 0.5, 1, 2, 3, and 4 years. The Luvisol trial started in April 2019 and sampling occurred every 0.5 year for 2.5 years.

2.3. X-ray Computed Tomography and subsampling

At each sampling date, the mesocosms were scanned with an industrial X-ray μCT device (X-Tek Systems Ltd; XT H 225, Nikon Metrology, Belgium). The samples from the Chernozem trial were scanned for 63 min using a 0.7 mm copper filter at 160 kV and 255 μA, resulting in 2700 projections (2 frames per projection, 0.708 s per projection). The energy settings for the Luvisol trial were 142 kV, 460 μA, and a 0.8 mm copper filter for reduction of beam hardening artefacts. A voxel size of 60 μm was achieved at an 8-bit greyscale resolution in the reconstructed tomograms. The smallest features that can be detected typically amount to twice the voxel size, i.e. 120 μm. After scanning, the tomograms of the three mesocosms per soil and treatment intended for subsampling were visually evaluated to identify prominent features to be included in subsamples. From each mesocosm, two subsamples (3 cm height, 3 cm diameter, 21 cm^3) were taken from 0 to 5 cm depth, using a sampling device for undisturbed subsampling (Umwelt-Geräte-Technik GmbH, Germany). To do so, the mesocosm was fixed and the soil core was gently pressed out of the cylinder from the bottom into the subsample cylinders by a stamp. The subsamples were scanned for 63 min at 130 kV and 150 μA using a 0.1-mm copper filter, resulting in 2,000 projections (0.708 s per projections, 2 frames per projection) and reconstructed with a voxel size of 15 μm (8-bit format).

2.4. Mesocosm analysis

The voxel size of mesocosm scans (60 μm) was too coarse to detect plant residues and garnet particles. Therefore, mesocosm scans were only subjected to pore space analysis and bioturbation rate analysis via detection of temporal changes. For pore space analysis, the images were first filtered with a non-local means filter implemented in FIJI ImageJ V1.53. Then, vertical differences in average image intensity were removed and pores were segmented using the average method of five commonly used automatic threshold detection methods based on the grey value histogram (Schlüter et al., 2014). Both methods are implemented in the QuantIm software package (Vogel et al., 2010). The pore space was analyzed with respect to visible porosity [mm^3 mm^{-3}], pore surface area density [mm^2 mm^{-3}], Euler number density [1 mm^{-3}], connection probability [–], mean pore distance [mm] and mean pore size [mm] according to a standard protocol (Weller et al., 2022) implemented in Fiji ImageJ (Schindelin et al., 2012) and associated plugins (Legland et al., 2016). The dimensionless connection probability, Γ, reflects the probability of two randomly chosen pore voxels to belong to the same pore cluster and was calculated by Equation (1):

$$\Gamma(p) = \frac{1}{n_p^2}\sum_{i=1}^{N(X_p)} x_i^2 \quad (1)$$

where n_p is the total number of pore voxels in the analyzed volume, X_p, and n_i is the number of pore voxels per cluster. The Euler number quantifies the connectivity as the number of isolated pores minus the number of redundant connections plus the number of cavities.

We further measured the volume fraction affected by bioturbation based on repeated scans of the same mesocosms. Scans of excavated mesocosms were registered to scans of their respective initial state via elastix image registration (Klein et al., 2010) and subtracted from each other with the Image Calculator in Fiji ImageJ. The difference image indicated regions where new pores were created or old pores were destroyed. Volume fractions of bioturbation regions were calculated by thresholding. In order to reduce image noise, a soil-specific threshold of 120 (Chernozem) and 80 (Luvisol) grey values was applied. Then the binary image was filtered with a 3D-median filter and objects < 1000 voxels were removed using connected components labelling in the MorpholobJ plugin for FIJI ImageJ (Legland et al., 2016). As a consequence, only features with diameters > 1.2 mm remained.

2.5. Subsample analysis

The voxel size of subsamples (15 μm) was sufficient to resolve individual garnet particles and particulate organic matter. The raw greyscale data was segmented into different material classes via supervised, machine-learning based image classification with the ilastik segmentation toolkit (Berg et al., 2019). The trained material classes were pores, particulate organic matter (roots, cocoons, plant residues), soil matrix, dense matter (including sand grains and iron-rich concretions), and

garnet particles (Fig. S2). A random forest classifier was trained on a number of attributes that included the grey value, the gradient (1st derivate of grey values), and texture information (2nd derivate of grey values) at different spatial scales and shape characteristics (Leuther et al., 2022; Schlüter et al., 2022). Two independent classifiers were trained for the two soils with subjectively compiled training data sets comprising 12 sub-volumes (400 × 400 × 400 voxel) that representatively captured the whole range of structural features observed in the X-ray μCT images. The training data set resulted in out-of-bag (OOB) estimate of error rates of < 1.5 %.

The pore space of the subsample scans was subjected to the same quantitative analysis as described for the mesocosm scans. The Euclidean distance transform of the pore space as implemented in Fiji ImageJ resulted in the shortest pore distance of every non-pore voxel. Only considering garnet particle voxels for averaging of these Euclidean distances resulted in the mean particle − pore distance. Including all soil matrix and dense material voxels for averaging resulted in the mean matrix − pore distance. The ratio of both distances was used to assess particle randomization and estimate soil structure turnover. The mean distance of garnet particles to the next pore is supposed to be minimal at the beginning and increases as soon as the particles leave their initial position at the aggregate surfaces (Fig. 1a), either by occlusion in between aggregates or by increasingly complete mixing processes (Fig. 1b). Complete randomization of garnet particles in the soil matrix will increase their average pore distances and adjust it to the average pore distance in soil (Fig. 1c). Progressing soil structure turnover, hence, drives the ratio of the two distances towards unity.

These distance ratios were determined for the entire volume of the subsamples but also for subjectively defined regions of interest affected by specific structural features (roots, casts, cocoons, and burrows). These features were segmented and used to create a region of interest to analyze their vicinities according to their region of impact. While earthworms created burrows affecting the surrounding soil to a distance of around 2 mm, the impact zone of grass roots was around 0.5 mm. Also, the embedment of macrofauna cocoons, being placed in-between cast, had an impact zone of approximately 0.5 mm distance.

2.6. Data analysis

Data management, data analysis, and preparation of graphs were done using the open source packages tidyverse (Wickham et al., 2019) and ggplot2 (Wickham, 2016) in R Version 4.0.5 (R Core Team, 2020). Structure development as function of time for individual treatments and sites was evaluated using analysis of variance (ANOVA). The *p* values of pairwise t-tests were adjusted using the Bonferroni multiple testing correction method. Data were tested for normality ($p > 0.01$) using Shapiro-Wilk Normality test and for variance homogeneity ($p > 0.05$) using Levene Test (Kassambara, 2020). Significance of ANOVA were post hoc-tested at $p < 0.05$. Soil structure properties determined for the mesocosms initially scanned (time point = 0 years) and those sampled, scanned, and reburied at every time point, were included in the analysis in order to increase the number of replicates, even though values are not independent. The connection probability (Γ) was log transformed before testing. The model error of the inverted linear model was used to determine the standard error in soil structure turnover times. Differences in biological features were tested by Kruskal-Wallis test with Bonferroni p-adjustment (de Mendiburu and Yaseen, 2020), because requirements for an ANOVA were not fulfilled.

3. Results

3.1. Soil structure changes within mesocosms

The capability of soil macrofauna to remodel soil structure was evident when comparing the initial states of mesocosms with those after two years exposure to field conditions (Fig. 2a, b). The initial structure after packing was characterized by a homogenous distribution of sieved and repacked aggregates and macropores between them. Garnet particles (size = 45–100 μm) were not visible at the coarse resolution used to scan the entire mesocosms (smallest detectable features > 120 μm). After two years, we observed new macropores partially filled with cast and compacted areas in the surroundings of new macropores. However, most areas appeared unaffected at this resolution, leading to only slight changes in pore network indicators of the mesocosms (Table S1). Those changes were mainly due to settlement in the first year and superimposed by earthworm burrows (3–9 mm width) in individual samples exposed to biota > 30 μm (Fig. S3a). Difference images of the initial structure and the structure after excavation showed that the change rate of the volume fraction affected by soil structure re-arrangement was on average 0.0032 $mm^3\ mm^{-3}\ year^{-1}$ for the Chernozem and 0.0067 $mm^3\ mm^{-3}\ year^{-1}$ for the Luvisol for mesocosms allowing for accesses for biota > 30 μm (Fig. S4). By taking the inverse (Sierra et al., 2017), the estimated apparent time for complete structure turnover was 149 years for the Luvisol and 316 years for the Chernozem. For mesocosms where activity of fauna and roots > 30 μm was excluded, and thus, mainly exposed to abiotic effects, negligible differences between initial and final scans were detected (<0.001 $mm^3\ mm^{-3}\ year^{-1}$). The spatial accuracy of these difference images, however, is rather low (>1.2 mm) and therefore does not capture all soil entities involved in soil structure turnover. Moreover, partial refilling of newly formed macropores with

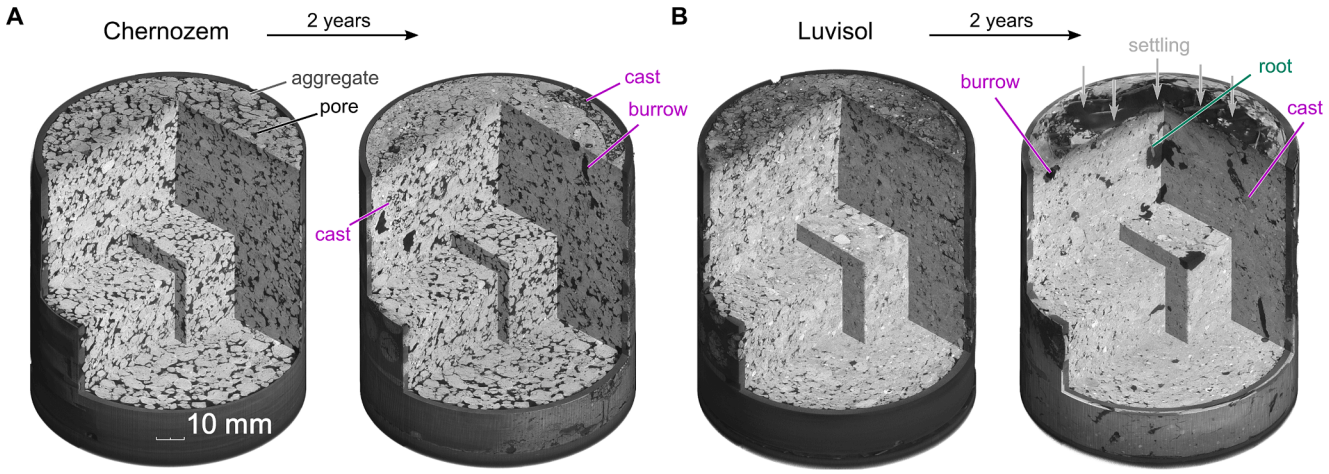

Fig. 2. X-ray μCT images of the mesocosms of the Chernozem (A) and Luvisol (B) scanned at 0.060-mm resolution as initially packed and after 2 years of exposure to abiotic and biotic turnover (with access for biota > 30 μm).

cast concealed the soil structure change that actually took place locally, which caused a bias towards longer apparent turnover times at the mm-cm scale.

Subsamples taken from the mesocosms allowed for scanning at higher resolution, and thus, the detection of smaller features (>30 μm), including individual garnet particles as well as traces of biotic activity. Most garnet particles remained at their initial location along aggregate surfaces and were only relocated in regions where bioturbation was evident. Macrofauna embedded cocoons in casts, produced burrows either empty or refilled with cast material, and completely rearranged the structure as indicated by the redistribution of garnet particles (Fig. 3a and b). However, the garnet particle density in casts was sometimes low, as the soil was partially incorporated from outside the mesocosms. Smaller biopores (0.05–0.2 mm width), likely formed by mesofauna, fragmented labelled aggregates without the displacement of garnet particles, and thus, changed pore architecture and pore distances only locally (Fig. 4b). Roots (0.1–0.8 mm width) occupied existing pores, grew along earthworm casts, but also created new pores by ingression into labelled aggregates.

The high-resolution scans were subjected to quantitative pore structure analysis (Table S2, Fig. 4) in order to compare the evolving pore structure to that of undisturbed reference topsoils serving as proxies for the site-specific dynamic equilibrium of soil structure. The indicators showed very similar pore characteristics for undisturbed soil at both sites, but differed significantly from the repacked structures ($p < 0.05$). For samples with access to biota > 30 μm, fauna and roots created biopores with larger pore diameters, partly replacing the initial structures, and causing the volume fraction of pores > 0.30 mm to increase (Fig. S3b). The pore size distributions kept changing even until the end of the study period, suggesting that soil structure still had not reached the site-specific equilibrium. This idea is supported by the different indicators of pore characteristics changing at site-specific rates. Pore characteristics of the repacked Chernozem differed most from the natural conditions (Fig. 4a, b, Table S2) and most of the indicators evolved towards the site-specific values during the 4 years. Biotic activity caused stronger changes in structural indicators and accelerated the structural development. The high variability in the pore indicators suggest that structure development was often depending on whether macrofauna burrows and casts were captured by the subsampling. For both treatments of the Luvisol mesocosms (with and without access for biota > 30 μm), indicators showed seasonal fluctuations around the values determined for undisturbed samples. During winter, mean pore size and mean pore distance increased, while pore surface density decreased (Fig. 4a, b, Table S2). For the treatment without access for biota > 30 μm, this was accompanied by a decrease in pores sizes close to the detection limit (Fig. S3b). During spring and summer, these indicators often returned to their initial values. These seasonal changes were most pronounced for the treatment without access for biota > 30 μm, indicating that mainly abiotic factors, such as more intense swelling of clay minerals in winter due to higher water contents, drove the reversible fluctuations. Still, the change in different indicators of pore characteristics does not allow for precise estimation of time until dynamic equilibrium is reached. This inherent limitation, however, can be overcome by mapping the redistribution of garnet particles within the soil pore space over time (Fig. 1).

3.2. Soil structure turnover determined by particle re-distribution

The initial packings and garnet particle location amounted to a mean ratio between particle – pore and matrix – pore distances of 0.39 to 0.42 mm mm^{-1} for both soils and treatments (measured after 0.5 years).

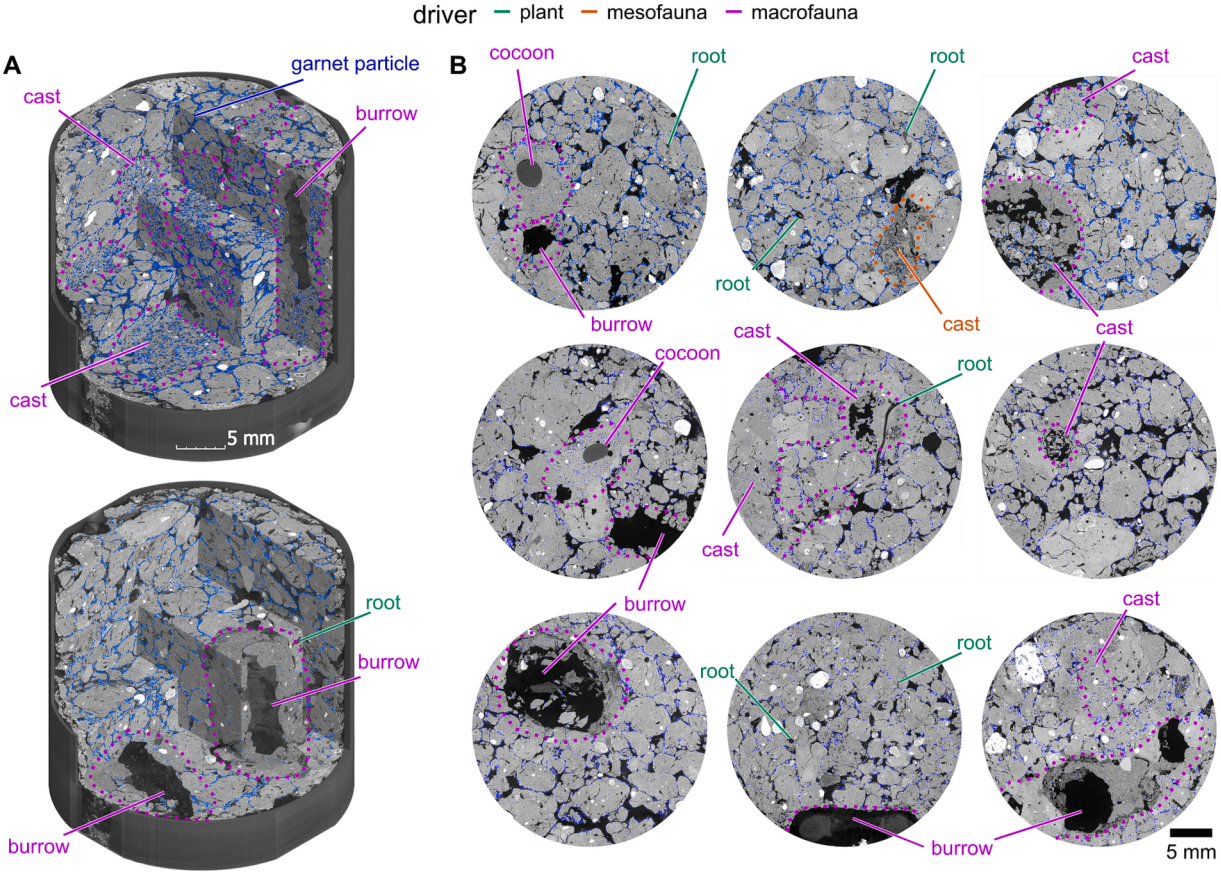

Fig. 3. X-ray μCT images of mesocosm subsamples. A. Tomogram of two subsamples with access for biota > 30 μm of the Luvisol trial and B. 2D horizontal slices of different biological features scanned at 0.015-mm resolution. Garnet particles are blue, dashed lines mark areas modified by bioturbation. (For interpretation of the references to colour in this figure legend, the reader is referred to the web version of this article.)

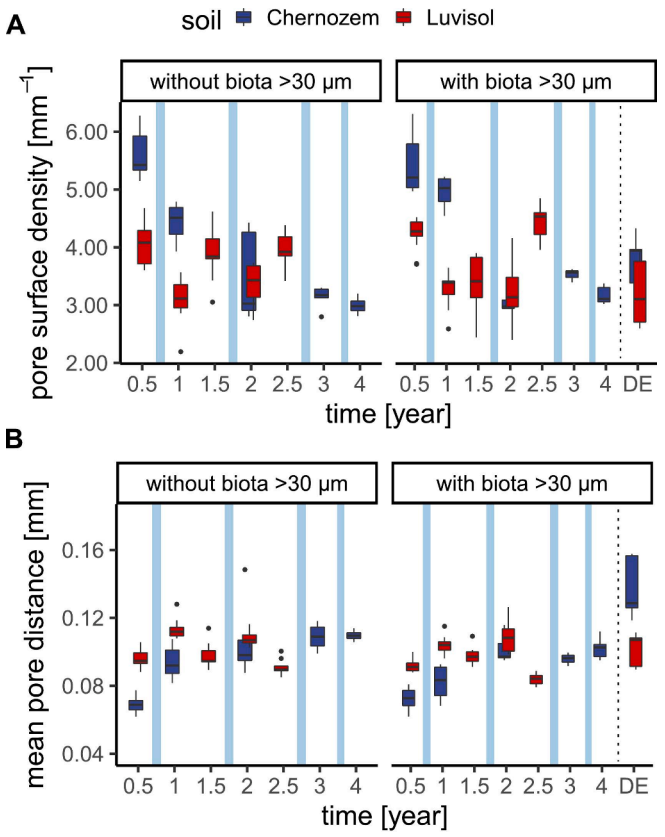

Fig. 4. Soil structural indicators of mesocosm subsamples. A depicts the development of the pore surface density over time, and B the mean pore distance of voxels classified as non-pore. The light blue areas in A and B mark the winter periods, the dashed line the results at dynamic equilibrium (DE) of soil structure (>60 years). Duration and sampling frequency differ between sites. (For interpretation of the references to colour in this figure legend, the reader is referred to the web version of this article.)

The initial mean ratio was not equal to 0, as a sizable amount of particles was occluded from visible pores at the contact zone between labelled aggregates with large distances to the next visible pore (Fig. 1, Fig. 3). The amounts of garnet particles determined per subsample remained constant throughout the experiments (4 to 6 vol-%), indicating stabile recovery rate and negligible particle loss, for example, by percolating water. During the first year, compaction by sample settling dominated the redistribution of particles, resulting in a shift of the ratio of the two distances parallel to the 1:1 line (Fig. 5a) for both trials and treatments. This is expected since the loss of visible pores did not only occlude garnet particles but also caused a concomitant increase in pore distances within the soil matrix. Driven by the settling-induced, strong increase in matrix − pore distances (Fig. 3d), the distance ratio for the Chernozem decreased to 0.34 mm mm^{-1} after 1 year for treatment with access for biota > 30 µm (Fig. 5b) and without (Fig. S5). Thereafter, the distance ratio increased continuously (Fig. 5b), indicating the dominance of true structure turnover as the decrease in particle − pore distance by new pore formation was smaller than the decrease in matrix − pore distances (Fig. 5a). For the Chernozem, linear regression of changes in distances ratios as a function of time revealed a randomization rate of 0.030 mm mm^{-1} year^{-1} for the treatment allowing for exposure to biotic effects (Fig. 5b) and of 0.018 mm mm^{-1} year^{-1} for the treatment exposed predominately to abiotic effects (Fig. S5). Estimated structure turnover times were 33 ± 3 (standard error) and 54 ± 6 years for the treatment with access for biota > 30 µm and without, respectively.

For the Luvisol treatment without access for biota > 30 µm, there was a small but continuous increase in the distances ratio with time that was superimposed by seasonal fluctuations, resulting in a randomization rate of 0.029 mm mm^{-1} year^{-1} (Fig. S5). Biological activity strongly enforced the randomization of garnet particles, causing steady increase in distances ratio with time and a randomization rate of 0.061 mm mm^{-1} year^{-1} (Fig. 5b). Structure turnover times were estimated to be 16 ± 1 and 34 ± 4 years for the treatment with access for biota > 30 µm and without, respectively.

Roots and earthworms were previously identified as the main drivers for changes in visible soil structure (Fig. 3a and b). The capability for particle redistribution, and hence, the turnover of soil structure, was therefore additionally analyzed in the direct vicinity of typical features

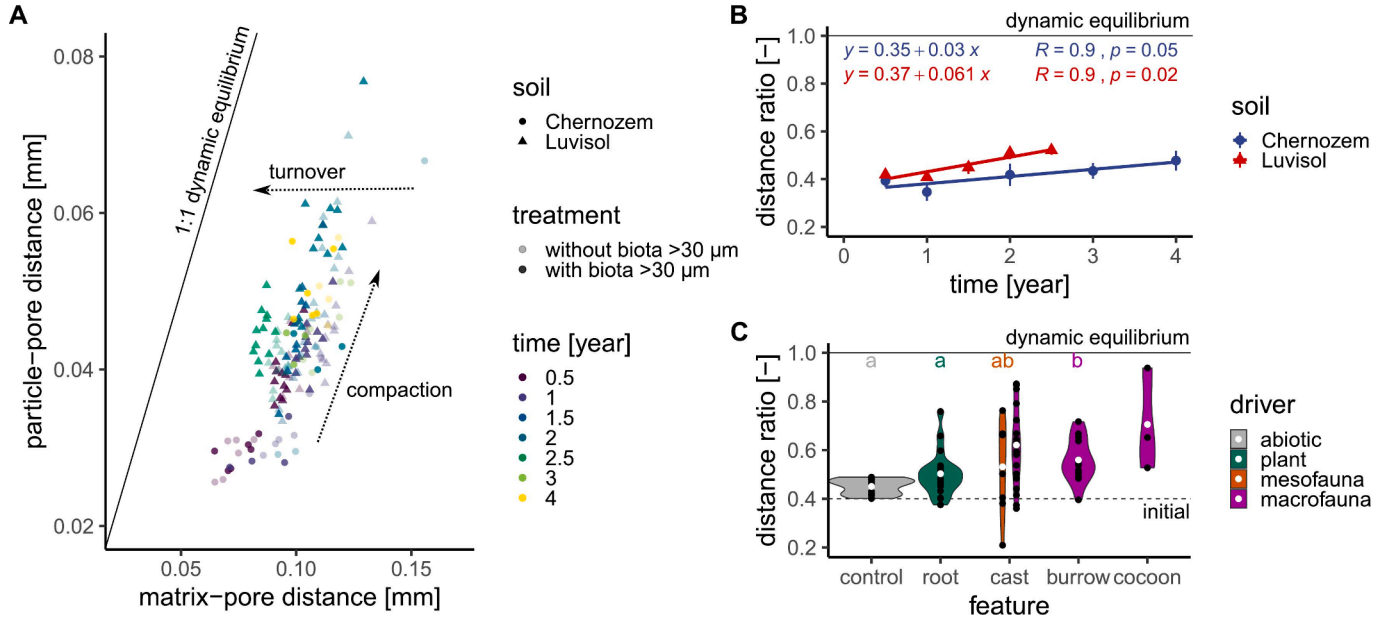

Fig. 5. Soil structure turnover determined by the distribution of garnet particles (size = 45–100 µm). A relation of particle − pore distance to matrix − pore distance determined for the 21-cm^3 subsamples. B mean distance ratio of the samples with access to biota > 30 µm as function of time. C shows the mean distance ratio of the samples without access to biota > 30 µm at the end of the experiments (control) and in the vicinity of structural features created by different biological drivers and their mean value (white dots). Small letters reflect significant differences between drivers tested at $p < 0.05$.

produced by fauna and roots (Fig. 3b). The selected regions had on average greater distances ratios (roots: 0.50 ± 0.02 mm mm^{-1}, mesofauna: 0.53 ± 0.07 mm mm^{-1}, macrofauna: 0.61 ± 0.02 mm mm^{-1}) than those of the treatments without access for biota > 30 μm at the end of the experiments (Chernozem: 0.44 mm mm^{-1} ± 0.01 se and Luvisol: 0.45 mm mm^{-1} ± 0.01 se) (Fig. 5c), yet only for macrofauna the difference was significant ($p < 0.001$).

4. Discussion

Our long-term monitoring of structure change in topsoils under grassland revealed the superposition of individual structure-forming processes that were previously mainly addressed individually, including settling of unconsolidated soils (Munkholm et al., 2008), periodic changes in pore structure upon wetting − drying cycles (Bodner et al., 2013; Cheik et al., 2021; Diel et al., 2019; Peng et al., 2007; Wang et al., 2017) and freeze − thaw cycles (Leuther and Schlüter, 2021; Ma et al., 2019; Miranda-Vélez et al., 2023; Starkloff et al., 2017), biopore formation by roots (Lucas et al., 2019b; Zhou et al., 2021) and soil fauna (Cheik et al., 2019; Mele et al., 2021) as well as associated compaction of the immediate vicinity (Capowiez et al., 2011; Lucas et al., 2019a), and production of cast of different size and densities by soil fauna (Briones, 2014; Le Bayon et al., 2021). Seasonal changes in structural indicators in both treatments indicate that the mesocosms were hydraulically well connected to the surrounding soil environment. The exclusion of roots by the 30 μm nylon gauze might have reduced the effect of drying compared to the samples with excess to roots.

The novel combination of long-term monitoring under field condition with soil structure labelling by inert garnet particles opened up completely new ways of characterizing soil structure turnover and providing space and time-resolved data needed for calibration of soil bioturbation models (Michel et al., 2022; Zech et al., 2022) and ecosystem models taking changes in carbon turnover and soil structure jointly into account (Meurer et al., 2020b). The randomization of inert particles integrates both abiotic and biotic processes over time, and thus, informs on the response of soil structure to environmental conditions. So far, the extrapolation based on turnover rates determined for up to four experimental years and assumes that randomization would progress linearly with exposure time. With surprising consistency, analyses at both the cm and μm scales indicated that the structure turnover time is two times faster in the Luvisol than the Chernozem topsoil. In addition, the turnover times derived from structure labelling revealed that these processes proceed over decades rather than years, which matches first simple model estimates of the time frame for restoration of disrupted pore structure by bioturbation (Meurer et al., 2020a).

Since soil texture and land use were similar at both sites, the different turnover times of 16 years for the moist Luvisol site and 33 years for the dry Chernozem site (Fig. 4b) indicate that the environmental conditions are important drivers of soil structure evolution. Grass roots had a minor impact on particle randomization because most root diameters did not exceed the available pore diameter and therefore tend to grow along existing pores, without inducing structural turnover (Lucas et al., 2019a). The impact of plant roots on soil structure turnover might be different under other land use systems or soil conditions, such as more compacted subsoils. When addressing these questions, a bulk density closer to 1.5 g cm^{-3} should be established in order to reduce the amount of well-connected macropores. Macrofauna activity appeared to be the major factor of particle redistribution (Capowiez et al., 2021; Heinze et al., 2021), as evidenced by the high degree of particle randomization in the surroundings of various biological features (Fig. 5c). Abundances of meso- and macrofauna being higher by several orders of magnitude were found for the Luvisol than the Chernozem (Scheunemann et al., 2010; Yin et al., 2019), with long dry spells being the most likely reason for the reduce bioturbation rates in the dry Chernozem topsoil (Ruiz et al., 2021). Exclusion of faunal activity > 30 μm slowed down the structure turnover by a factor of 1.6 for the Chernozem and factor 2.1 for the Luvisol, which underlines the paramount role of biotic drivers regarding the formation of structure in topsoils, and thus, their relevance to different soil functions (Vogel et al., 2022). The determined randomization rates due to abiotic processes might have even been overestimated due to possible effects of meso- and microfauna, roots, and fungal hyphae smaller than the nylon mesh size of < 30 μm. In turn, the partial shielding of the mesocosms by perforated walls and the removal of plant residues from repacked soils might have somewhat reduced soil structure turnover in the treatments with access for biota > 30 μm as compared to natural reference soil. In the future, the combination of long-term soil structure monitoring and structure labelling can be utilized for determining soil structure turnover times across biomes and land uses, in order to improve ecosystem models operating at the continental to global scale. Such monitoring campaigns can be standardized and maintain at relatively low cost and can be conducted as coordinated, distributed field experiments (Borer et al., 2014; Keuskamp et al., 2013).

The other major benefit of estimates of soil structure turnover time is that they provide truly complementary information on fundamental processes that govern carbon sequestration in soil, such as the physical protection of organic matter. This is a considerable improvement over the indirect deduction of soil structure evolution and aggregate turnover estimated from carbon turnover rates (Amelung et al., 2008; Jastrow et al., 2007; Totsche et al., 2018), where results can be biased by uncertainties resulting from the use of different organic carbon and aggregate fractionation methods (Beare and Bruce, 1993; Poeplau et al., 2018). The selected scale at which garnet particles were tracked by X-ray μCT was just about right to detect the pore size range of 30–150 μm that is deemed most relevant for microbial activity as well as carbon turnover (Kravchenko et al., 2019). Hence, the redistribution of particles within the soil matrix is a good approximation of how particulate organic matter (POM) becomes occluded or exposed to pores, or how mineral-associated organic matter (MAOM) is subjected to changing micro-environmental conditions (Fig. 6). Stabile isotope analysis showed that the turnover times of POM and MAOM in topsoil of temperate ecosystems range from a few years to decades and centuries, respectively (Georgiou et al., 2022; Shi et al., 2020; von Lützow et al., 2007). Previous studies on long-term continuous maize cultivation experiments in direct vicinity of the Luvisol grassland (<0.1 km away) and Chernozem grassland (Phaeozem with slightly coarser soil texture, 15 km away) revealed average carbon turnover time of plant-derived POM within the topsoil of 54 years for the Luvisol and around 114 years for the Phaeozem (Flessa et al., 2008; John et al., 2005; Rethemeyer, 2004). At both sites, the turnover times of different organic matter fractions were in the order free POM (Luvisol: 22 years, Phaeozem: 52 years) < occluded POM (Luvisol: 49 years, Phaeozem: 83 years) < MAOM (Luvisol: 63 years, Phaeozem: 126 years). Similar to soil structure turnover time, the turnover times of the individual organic matter fractions were about a factor two slower in the dry region of the Chernozem site than in the moist region of the Luvisol, indicating more favorable conditions for mineralization under moist conditions.

The estimated soil structure turnover times were more similar to free POM turnover times than to those of MAOM (Fig. 6). With our experimental design we cannot clarify whether soil structure turnover directly governed POM turnover or whether they just happen to take place at the same pace. Future studies employing simultaneous labelling of soil structure and organic matter could provide direct information on the link between their turnover. Yet, the general congruency of free POM turnover and structure turnover times suggests that there is a reasonable possibility of fresh organic matter, such as root and litter fragments, to be translocated to microenvironments where mineralization is slower than at its initial position (Ortega-Ramírez et al., 2023; Schlüter et al., 2022). However, part of the fresh plant debris might be decomposed before becoming occluded during soil structure turnover (Berthelin et al., 2022; Hättenschwiler et al., 2005; Silver and Miya, 2001). Indeed, it was shown previously that only 15 (Luvisol) to 30 % (Phaeozem) of

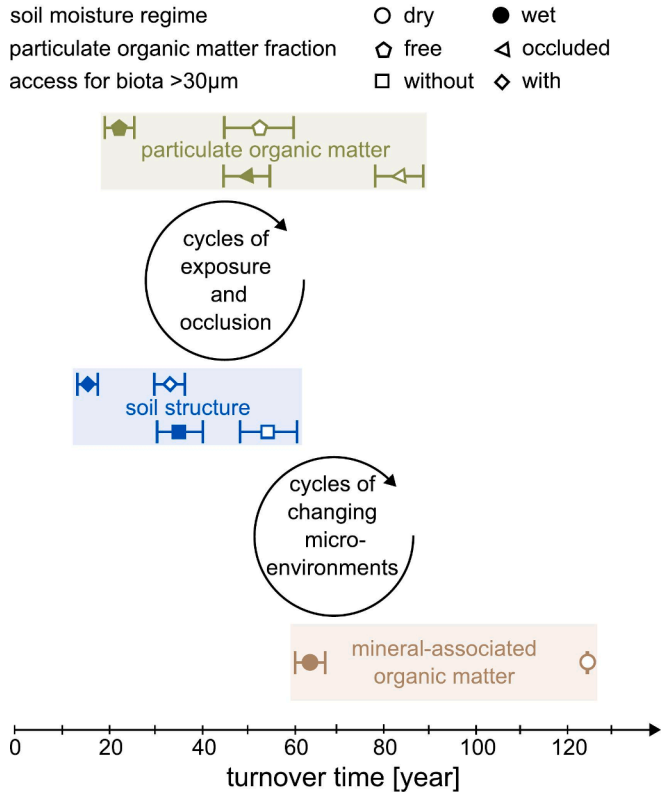

Fig. 6. Soil structure turnover and its impact on organic matter turnover. Soil structure turnover induces cycles of occlusion and exposure of particulate organic matter (POM) and cycles of changing microenvironments for mineral-associated organic matter (MAOM). POM and MAOM turnover times and their standard error were derived from literature based on nearby sites (Flessa et al., 2008; John et al., 2005; Rethemeyer, 2004).

the total input of fresh maize carbon was stored in soil (Flessa et al., 2008; John et al., 2005) while the rest was mineralized in short term. In contrast, MAOM may survive several exposure cycles before becoming mineralized or exchanged for younger organic carbon (Fig. 6) (Leinemann et al., 2018). The substantially slower turnover of occluded POM and MAOM than the determined structural turnover suggests that the physical protection is only one mechanism retarding organic matter mineralization next to stabilization on mineral surfaces, low-energy gain by microorganisms imposed by physico-chemical conditions or organic matter quality, and others (Keiluweit et al., 2016; Schmidt et al., 2011).

In summary, structure turnover within decades prevents extensive protection of fresh organic matter from microbial degradation, but the structure remains stable long enough to allow the soil matrix to be become enriched in MAOM in the vicinity of POM upon uptake of degradation products (Quigley et al., 2018; Schlüter et al., 2022; Witzgall et al., 2021) or carbon-depleted at the surfaces of aerated pores due to accelerated microbial mineralization (Schlüter et al., 2022). In turn, very fast structure turnover in the range of primary production, e.g. 1–2 years, might cause enrichment of carbon in topsoil by occlusion of POM and facilitate MAOM formation in the soil matrix, thus likely increasing overall soil carbon persistency.

5. Conclusions

The combination of field-exposure of mesocosms, structure labelling, and X-ray µCT enabled to assess soil structure turnover time under field conditions. Turnover time was 16 years under moist conditions (Luvisol) and 33 years under dry climate (Chernozem). Long dry spells during the experimental period likely reduced bioturbation and slowed down the development of soil structure towards its site-specific dynamic equilibrium. We found that freeze – thaw and wetting – drying cycles caused seasonal fluctuations in structure. These were mostly reversible and contributed little to the incorporation of garnet particles into the soil matrix. Biological activity, in contrast, induced irreversible soil structure turnover as revealed by particle randomisation with respect to pore distances. The structure turnover times were in accordance to turnover times of particulate organic matter previously determined on nearby sites, indicating a possible link between soil structure evolution and physical protection of organic matter in soil. The combination of structure labelling with long-term monitoring of field mesocosms therefore holds great potential in exploring the contribution of soil structure to carbon sequestration.

Declaration of Competing Interest

The authors declare the following financial interests/personal relationships which may be considered as potential competing interests: Frederic Leuther reports financial support was provided by German Research Foundation.

Acknowledgment

We thank the Research Station Bad Lauchstädt and the Höhere Landbauschule Rotthalmünster for access to field sites and maintenance of the trials.

Funding

German Research Foundation grant no. 416883305.

Data availability

The source data underlying Figs. 3–4 as well as Supplementary Figs. 2–4 and Table 1–2 are provided in this paper. Segmented X-ray µCT data of cylinders at dynamic equilibrium will be uploaded at the Soil Structure Library hosted by the UFZ (https://structurelib.ufz.de/). Additional image data, as well as image analysis codes, are available from the authors upon request.

Appendix A. Supplementary data

Supplementary data to this article can be found online at https://doi.org/10.1016/j.geoderma.2023.116464.

References

Altermann, M., Rinklebe, J., Merbach, I., Körschens, M., Langer, U., Hofmann, B., 2005. Chernozem—soil of the year 2005. J. Soil Sci. Plant Nutr. 168, 725–740. https://doi.org/10.1002/jpln.200521814.

Amelung, W., Brodowski, S., Sandhage-Hofmann, A., Bol, R., 2008. Combining biomarker with stable isotope analyses for assessing the transformation and turnover of soil organic matter. Adv. Agron. 100, 155–250. https://doi.org/10.1016/S0065-2113(08)00606-8.

Beare, M.H., Bruce, R.R., 1993. In: Soil Structure/Soil Biota Interrelationships. Elsevier, pp. 87–104.

Berg, S., Kutra, D., Kroeger, T., Straehle, C.N., Kausler, B.X., Haubold, C., Schiegg, M., Ales, J., Beier, T., Rudy, M., Eren, K., Cervantes, J.I., Xu, B., Beuttenmueller, F., Wolny, A., Zhang, C., Koethe, U., Hamprecht, F.A., Kreshuk, A., 2019. ilastik: interactive machine learning for (bio)image analysis. Nat. Methods 16 (12), 1226–1232.

Berthelin, J., Laba, M., Lemaire, G., Powlson, D., Tessier, D., Wander, M., Baveye, P.C., 2022. Soil carbon sequestration for climate change mitigation: Mineralization kinetics of organic inputs as an overlooked limitation. Eur. J. Soil. Sci. 73 (1), e13221. https://doi.org/10.1111/ejss.13221.

Bodner, G., Scholl, P., Kaul, H.P., 2013. Field quantification of wetting–drying cycles to predict temporal changes of soil pore size distribution. Soil Tillage Res. 133, 1–9. https://doi.org/10.1016/j.still.2013.05.006.

Borer, E.T., Harpole, W.S., Adler, P.B., Lind, E.M., Orrock, J.L., Seabloom, E.W., Smith, M.D., Freckleton, R., 2014. Finding generality in ecology: a model for globally distributed experiments. Methods Ecol. Evol. 5 (1), 65–73.

Bottinelli, N., Jouquet, P., Capowiez, Y., Podwojewski, P., Grimaldi, M., Peng, X., 2015. Why is the influence of soil macrofauna on soil structure only considered by soil

ecologists? Soil Tillage Res. 146, 118–124. https://doi.org/10.1016/j.still.2014.01.007.
Briones, M.J.I., 2014. Soil fauna and soil functions: a jigsaw puzzle. Front. Environ. Sci. 2 https://doi.org/10.3389/fenvs.2014.00007.
Capowiez, Y., Sammartino, S., Michel, E., 2011. Using X-ray tomography to quantify earthworm bioturbation non-destructively in repacked soil cores. Geoderma 162, 124–131. https://doi.org/10.1016/j.geoderma.2011.01.011.
Capowiez, Y., Gilbert, F., Vallat, A., Poggiale, J.-C., Bonzom, J.-M., 2021. Depth distribution of soil organic matter and burrowing activity of earthworms—mesocosm study using X-ray tomography and luminophores. Biol. Fertil. Soils 57, 337–346. https://doi.org/10.1007/s00374-020-01536-y.
Cheik, S., Bottinelli, N., Minh, T.T., Doan, T.T., Jouquet, P., 2019. Quantification of three dimensional characteristics of macrofauna macropores and their effects on soil hydraulic conductivity in Northern Vietnam. Front. Environ. Sci. 7 https://doi.org/10.3389/fenvs.2019.00031.
Cheik, S., Jouquet, P., Maeght, J.-L., Capowiez, Y., Tran, T.M., Bottinelli, N., 2021. X-ray tomography analysis of soil biopores structure under wetting and drying cycles. Eur. J. Soil. Sci. 72, 2128–2132. https://doi.org/10.1111/ejss.13119.
Coleman, D.C., Callaham, M., Crossley Jr, D., 2017. Fundamentals of soil ecology. Academic Press.
De Gryze, S., Six, J., Merckx, R., 2006. Quantifying water-stable soil aggregate turnover and its implication for soil organic matter dynamics in a model study. Eur. J. Soil. Sci. 57, 693–707. https://doi.org/10.1111/j.1365-2389.2005.00760.x.
de Mendiburu, F., Yaseen, M., 2020. agricolae: Statistical Procedures for Agricultural Research. Version, R Package, pp. 1–2.
Diel, J., Vogel, H.-J., Schlüter, S., 2019. Impact of wetting and drying cycles on soil structure dynamics. Geoderma 345, 63–71. https://doi.org/10.1016/j.geoderma.2019.03.018.
Don, A., Steinberg, B., Schöning, I., Pritsch, K., Joschko, M., Gleixner, G., Schulze, E.-D., 2008. Organic carbon sequestration in earthworm burrows. Soil Biol. Biochem. 40 (7), 1803–1812.
Erktan, A., Or, D., Scheu, S., 2020. The physical structure of soil: determinant and consequence of trophic interactions. Soil Biol. Biochem. 148, 107876. https://doi.org/10.1016/j.soilbio.2020.107876.
Flessa, H., Amelung, W., Helfrich, M., Wiesenberg, G.L.B., Gleixner, G., Brodowski, S., Rethemeyer, J., Kramer, C., Grootes, P.M., 2008. Storage and stability of organic matter and fossil carbon in a Luvisol and Phaeozem with continuous maize cropping: a synthesis. J. Soil Sci. Plant Nutr 171 (1), 36–51.
Garbout, A., Munkholm, L.J., Hansen, S.B., 2013. Temporal dynamics for soil aggregates determined using X-ray CT scanning. Geoderma 204–205, 15–22. https://doi.org/10.1016/j.geoderma.2013.04.004.
Georgiou, K., Jackson, R.B., Vindušková, O., Abramoff, R.Z., Ahlström, A., Feng, W., Harden, J.W., Pellegrini, A.F.A., Polley, H.W., Soong, J.L., Riley, W.J., Torn, M.S., 2022. Global stocks and capacity of mineral-associated soil organic carbon. Nat. Commun. 13 (1) https://doi.org/10.1038/s41467-022-31540-9.
Grosse, M., Hierold, W., Ahlborn, M.C., Piepho, H.-P., Helming, K., 2020. Long-term field experiments in Germany: classification and spatial representation. Soil 6, 579–596. https://doi.org/10.5194/soil-6-579-2020.
Hättenschwiler, S., Tiunov, A.V., Scheu, S., 2005. Biodiversity and litter decomposition in terrestrial ecosystems. Annu. Rev. Ecol. Evol. Syst. 36, 191–218. https://doi.org/10.1146/annurev.ecolsys.36.112904.151932.
Heinze, W.M., Mitrano, D.M., Lahive, E., Koestel, J., Cornelis, G., 2021. Nanoplastic transport in soil via bioturbation by Lumbricus terrestris. Environ. Sci. Technol. 55, 16423–16433. https://doi.org/10.1021/acs.est.1c05614.
Hinsinger, P., Bengough, A.G., Vetterlein, D., Young, I.M., 2009. Rhizosphere: biophysics, biogeochemistry and ecological relevance. Plant Soil 321, 117–152. https://doi.org/10.1007/s11104-008-9885-9.
Jastrow, J.D., Amonette, J.E., Bailey, V.L., 2007. Mechanisms controlling soil carbon turnover and their potential application for enhancing carbon sequestration. Clim. Change 80, 5–23. https://doi.org/10.1007/s10584-006-9178-3.
John, B., Yamashita, T., Ludwig, B., Flessa, H., 2005. Storage of organic carbon in aggregate and density fractions of silty soils under different types of land use. Geoderma 128, 63–79. https://doi.org/10.1016/j.geoderma.2004.12.013.
Kassambara, A., 2020. rstatix: pipe-friendly framework for basic statistical tests. https://CRAN.R-project.org/package=rstatix.
Keiluweit, M., Nico, P.S., Kleber, M., Fendorf, S., 2016. Are oxygen limitations under recognized regulators of organic carbon turnover in upland soils? Biogeochemistry 127, 157–171. https://doi.org/10.1007/s10533-015-0180-6.
Keiluweit, M., Wanzek, T., Kleber, M., Nico, P., Fendorf, S., 2017. Anaerobic microsites have an unaccounted role in soil carbon stabilization. Nat. Commun. 8, 1–10. https://doi.org/10.1038/s41467-017-01406-6.
Keller, T., Colombi, T., Ruiz, S., Schymanski, S.J., Weisskopf, P., Koestel, J., Sommer, M., Stadelmann, V., Breitenstein, D., Kirchgessner, N., Walter, A., Or, D., 2021. Soil structure recovery following compaction: short-term evolution of soil physical properties in a loamy soil. Soil Sci. Soc. Am. J. 85 (4), 1002–1020.
Keuskamp, J.A., Dingemans, B.J.J., Lehtinen, T., Sarneel, J.M., Hefting, M.M., Muller-Landau, H., 2013. Tea Bag Index: a novel approach to collect uniform decomposition data across ecosystems. Methods Ecol. Evol. 4 (11), 1070–1075.
Klein, S., Staring, M., Murphy, K., Viergever, M.A., Pluim, J.P., 2010. Elastix: a toolbox for intensity-based medical image registration. IEEE Trans. Med. Imaging 29, 196–205. https://doi.org/10.1109/TMI.2009.2035616.
Koestel, J., Schlüter, S., 2019. Quantification of the structure evolution in a garden soil over the course of two years. Geoderma 338, 597–609. https://doi.org/10.1016/j.geoderma.2018.12.030.
Kögel-Knabner, I., Ekschmitt, K., Flessa, H., Guggenberger, G., Matzner, E., Marschner, B., von Lützow, M., 2008. An integrative approach of organic matter stabilization in temperate soils: linking chemistry, physics, and biology. J. Soil Sci. Plant Nutr. 171 (1), 5–13.
Kravchenko, A., Guber, A., Razavi, B., Koestel, J., Quigley, M., Robertson, G., et al., 2019. Microbial spatial footprint as a driver of soil carbon stabilization. Nat. Commun. 10, 1–10. https://doi.org/10.1038/s41467-019-11057-4.
Le Bayon, R.-C., Guenat, C., Schlaepfer, R., Fischer, F., Luiset, A., Schomburg, A., Turberg, P., 2021. Use of X-ray microcomputed tomography for characterizing earthworm-derived belowground soil aggregates. Eur. J. Soil. Sci. 72 (3), 1113–1127.
Legland, D., Arganda-Carreras, I., Andrey, P., 2016. MorphoLibJ: integrated library and plugins for mathematical morphology with Image. J. Bioinform. 32, 3532–3534. https://doi.org/10.1093/bioinformatics/btw413.
Lehmann, J., Kleber, M., 2015. The contentious nature of soil organic matter. Nature 528, 60–68. https://doi.org/10.1038/nature16069.
Leinemann, T., Preusser, S., Mikutta, R., Kalbitz, K., Cerli, C., Höschen, C., Mueller, C.W., Kandeler, E., Guggenberger, G., 2018. Multiple exchange processes on mineral surfaces control the transport of dissolved organic matter through soil profiles. Soil Biol. Biochem. 118, 79–90.
Leuther, F., Schlüter, S., 2021. Impact of freeze–thaw cycles on soil structure and soil hydraulic properties. Soil 7, 179–191. https://doi.org/10.5194/soil-7-179-2021.
Leuther, F., Wolff, M., Kaiser, K., Schumann, L., Merbach, I., Mikutta, R., Schlüter, S., 2022. Response of subsoil organic matter contents and physical properties to long-term, high-rate farmyard manure application. Eur. J. Soil. Sci. 73 (2), e13233. https://doi.org/10.1111/ejss.13233.
Liu, S., Guo, Z.C., Pan, Y.B., Zhang, L.L., Hallett, P.D., Peng, X.H., 2019. Rare earth oxides for labelling soil aggregate turnover: impacts of soil properties, labelling method and aggregate structure. Geoderma 351, 36–48. https://doi.org/10.1016/j.geoderma.2019.05.015.
Lucas, M., Schlüter, S., Vogel, H.-J., Vetterlein, D., 2019a. Roots compact the surrounding soil depending on the structures they encounter. Sci. Rep. 9, 1–13. https://doi.org/10.1038/s41598-019-52665-w.
Lucas, M., Schlüter, S., Vogel, H.-J., Vetterlein, D., 2019b. Soil structure formation along an agricultural chronosequence. Geoderma 350, 61–72. https://doi.org/10.1016/j.geoderma.2019.04.041.
Ma, Q., Zhang, K., Jabro, J.D., Ren, L., Liu, H., 2019. Freeze–thaw cycles effects on soil physical properties under different degraded conditions in Northeast China. Environ. Earth Sci. 78, 1–12. https://doi.org/10.1007/s12665-019-8323-z.
Mele, G., Buscemi, G., Gargiulo, L., Terribile, F., 2021. Soil burrow characterization by 3D image analysis: prediction of macroinvertebrate groups from biopore size distribution parameters. Geoderma 404, 115292. https://doi.org/10.1016/j.geoderma.2021.115292.
Meurer, K., Barron, J., Chenu, C., Coucheney, E., Fielding, M., Hallett, P., Herrmann, A.M., Keller, T., Koestel, J., Larsbo, M., Lewan, E., Or, D., Parsons, D., Parvin, N., Taylor, A., Vereecken, H., Jarvis, N., 2020a. A framework for modelling soil structure dynamics induced by biological activity. Glob. Chang. Biol. 26 (10), 5382–5403.
Meurer, K.H.E., Chenu, C., Coucheney, E., Herrmann, A.M., Keller, T., Kätterer, T., Nimblad Svensson, D., Jarvis, N., 2020b. Modelling dynamic interactions between soil structure and the storage and turnover of soil organic matter. Biogeosciences 17 (20), 5025–5042.
Michel, E., Néel, M.-C., Capowiez, Y., Sammartino, S., Lafolie, F., Renault, P., et al., 2022. Making waves: modeling bioturbation in soils – are we burrowing in the right direction? Water Resour. Res. 216 https://doi.org/10.1016/j.watres.2022.118342.
Miranda-Vélez, J.F., Leuther, F., Köhne, J.M., Munkholm, L.J., Vogeler, I., 2023. Effects of freeze-thaw cycles on soil structure under different tillage and plant cover management practices. Soil Tillage Res. 225, 105540. https://doi.org/10.1016/j.still.2022.105540.
Munkholm, L.J., Hansen, E.M., Olesen, J.E., 2008. The effect of tillage intensity on soil structure and winter wheat root/shoot growth. Soil Use Manag. 24, 392–400. https://doi.org/10.1111/j.1475-2743.2008.00179.x.
Murphy, D.V., Recous, S., Stockdale, E.A., Fillery, I.R.P., Jensen, L.S., Hatch, D.J., et al., 2003. Gross nitrogen fluxes in soil: Theory, measurement and application of N-15 pool dilution techniques. In: Sparks, D.L. (Ed.), Adv. Agron. 79, pp. 69–118. https://doi.org/10.1016/s0065-2113(02)79002-0.
Nunan, N., Leloup, J., Ruamps, L.S., Pouteau, V., Chenu, C., 2017. Effects of habitat constraints on soil microbial community function. Sci. Rep. 7, 4280. https://doi.org/10.1038/s41598-017-04485-z.
Ortega-Ramírez, P., Pot, V., Laville, P., Schlüter, S., Amor-Quiroz, D.A., Hadjar, D., et al., 2023. Pore distances of particulate organic matter predict N2O emissions from intact soil at moist conditions. Geoderma 429, 116224. https://doi.org/10.1016/j.geoderma.2022.116224.
Peng, X., Horn, R., Smucker, A., 2007. Pore shrinkage dependency of inorganic and organic soils on wetting and drying cycles. Soil Sci. Soc. Am. J. 71, 1095–1104. https://doi.org/10.2136/sssaj2006.0156.
Plante, A.F., Feng, Y., McGill, W.B., 2002. A modeling approach to quantifying soil macroaggregate dynamics. Can. J. Soil. Sci. 82, 181–190. https://doi.org/10.4141/s01-024.
Poeplau, C., Don, A., Six, J., Kaiser, M., Benbi, D., Chenu, C., Cotrufo, M.F., Derrien, D., Gioacchini, P., Grand, S., Gregorich, E., Griepentrog, M., Gunina, A., Haddix, M., Kuzyakov, Y., Kühnel, A., Macdonald, L.M., Soong, J., Trigalet, S., Vermeire, M.-L., Rovira, P., van Wesemael, B., Wiesmeier, M., Yeasmin, S., Yevdokimov, I., Nieder, R., 2018. Isolating organic carbon fractions with varying turnover rates in temperate agricultural soils – a comprehensive method comparison. Soil Biol. Biochem. 125, 10–26.

Quigley, M.Y., Rivers, M.L., Kravchenko, A.N., 2018. Patterns and sources of spatial heterogeneity in soil matrix from contrasting long term management practices. Front. Environ. Sci. 6. https://doi.org/10.3389/fenvs.2018.00028.
R Core Team, 2020. R: A language and environment for statistical computing. R Foundation for Statistical Computing, Vienna, Austria.
Rabot, E., Wiesmeier, M., Schlüter, S., Vogel, H.-J., 2018. Soil structure as an indicator of soil functions: a review. Geoderma 314, 122–137. https://doi.org/10.1016/j.geoderma.2017.11.009.
Rethemeyer, J., 2004. Organic carbon transformation in agricultural soils: radiocarbon analysis of organic matter fractions and biomarker compounds. Christian-Albrecht-University, Kiel. Dissertation.
Ruamps, L.S., Nunan, N., Chenu, C., 2011. Microbial biogeography at the soil pore scale. Soil Biol. Biochem. 43, 280–286. https://doi.org/10.1016/j.soilbio.2010.10.010.
Ruiz, S.A., Bickel, S., Or, D., 2021. Global earthworm distribution and activity windows based on soil hydromechanical constraints. Commun. Biol. 4, 612. https://doi.org/10.1038/s42003-021-02139-5.
Scheunemann, N., Scheu, S., Butenschoen, O., 2010. Incorporation of decade old soil carbon into the soil animal food web of an arable system. Appl. Soil Ecol. 46, 59–63. https://doi.org/10.1016/j.apsoil.2010.06.014.
Schindelin, J., Arganda-Carreras, I., Frise, E., Kaynig, V., Longair, M., Pietzsch, T., Preibisch, S., Rueden, C., Saalfeld, S., Schmid, B., Tinevez, J.-Y., White, D.J., Hartenstein, V., Eliceiri, K., Tomancak, P., Cardona, A., 2012. Fiji: an open-source platform for biological-image analysis. Nat. Methods 9 (7), 676–682.
Schlüter, S., Vogel, H.-J., 2016. Analysis of soil structure turnover with garnet particles and X-ray microtomography. PLoS One 11, e0159948. https://doi.org/10.1371/journal.pone.0159948.
Schlüter, S., Sheppard, A., Brown, K., Wildenschild, D., 2014. Image processing of multiphase images obtained via X-ray microtomography: a review. Water Resour. Res. 50, 3615–3639. https://doi.org/10.1002/2014WR015256.
Schlüter, S., Leuther, F., Albrecht, L., Hoeschen, C., Kilian, R., Surey, R., Mikutta, R., Kaiser, K., Mueller, C.W., Vogel, H.-J., 2022. Microscale carbon distribution around pores and particulate organic matter varies with soil moisture regime. Nat. Commun. 13 (1) https://doi.org/10.1038/s41467-022-29605-w.
Schmidt, M.W.I., Torn, M.S., Abiven, S., Dittmar, T., Guggenberger, G., Janssens, I.A., Kleber, M., Kögel-Knabner, I., Lehmann, J., Manning, D.A.C., Nannipieri, P., Rasse, D.P., Weiner, S., Trumbore, S.E., 2011. Persistence of soil organic matter as an ecosystem property. Nature 478 (7367), 49–56.
Shi, Z., Allison, S.D., He, Y., Levine, P.A., Hoyt, A.M., Beem-Miller, J., Zhu, Q., Wieder, W.R., Trumbore, S., Randerson, J.T., 2020. The age distribution of global soil carbon inferred from radiocarbon measurements. Nat. Geosci. 13 (8), 555–559.
Sierra, C.A., Müller, M., Metzler, H., Manzoni, S., Trumbore, S.E., 2017. The muddle of ages, turnover, transit, and residence times in the carbon cycle. Glob. Chang. Biol. 23, 1763–1773. https://doi.org/10.1111/gcb.13556.
Silver, W.L., Miya, R.K., 2001. Global patterns in root decomposition: comparisons of climate and litter quality effects. Oecologia 129, 407–419. https://doi.org/10.1007/s004420100740.
Starkloff, T., Larsbo, M., Stolte, J., Hessel, R., Ritsema, C., 2017. Quantifying the impact of a succession of freezing-thawing cycles on the pore network of a silty clay loam and a loamy sand topsoil using X-ray tomography. Catena 156, 365–374. https://doi.org/10.1016/j.catena.2017.04.026.
Strong, D.T., Wever, H.D., Merckx, R., Recous, S., 2004. Spatial location of carbon decomposition in the soil pore system. Eur. J. Soil. Sci. 55, 739–750. https://doi.org/10.1111/j.1365-2389.2004.00639.x.
Totsche, K.U., Amelung, W., Gerzabek, M.H., Guggenberger, G., Klumpp, E., Knief, C., Lehndorff, E., Mikutta, R., Peth, S., Prechtel, A., Ray, N., Kögel-Knabner, I., 2018. Microaggregates in soils. J. Soil Sci. Plant Nutr 181 (1), 104–136.
Vogel, H.-J., Balseiro-Romero, M., Kravchenko, A., Otten, W., Pot, V., Schlüter, S., Weller, U., Baveye, P.C., 2022. A holistic perspective on soil architecture is needed as a key to soil functions. Eur. J. Soil. Sci. 73 (1), e13152. https://doi.org/10.1111/ejss.13152.
Vogel, H.J., Weller, U., Schlüter, S., 2010. Quantification of soil structure based on Minkowski functions. Comput. Geosci. 36, 1236–1245. https://doi.org/10.1016/j.cageo.2010.03.007.
von Lützow, M., Kögel-Knabner, I., Ekschmitt, K., Flessa, H., Guggenberger, G., Matzner, E., Marschner, B., 2007. SOM fractionation methods: relevance to functional pools and to stabilization mechanisms. Soil Biol. Biochem. 39 (9), 2183–2207.
Wang, C., Zhang, Z.-y., Liu, Y., Fan, S.-m., 2017. Geometric and fractal analysis of dynamic cracking patterns subjected to wetting-drying cycles. Soil Tillage Res. 170, 1–13. https://doi.org/10.1016/j.still.2017.02.005.
Weller, U., Albrecht, L., Schlüter, S., Vogel, H.J., 2022. An open soil structure library based on X-ray CT data. Soil 8, 507–515. https://doi.org/10.5194/soil-8-507-2022.
Wickham, H., 2016. ggplot2: elegant graphics for data analysis. Springer Cham.
Wickham, H., Averick, M., Bryan, J., Chang, W., McGowan, L., François, R., Grolemund, G., Hayes, A., Henry, L., Hester, J., Kuhn, M., Pedersen, T., Miller, E., Bache, S., Müller, K., Ooms, J., Robinson, D., Seidel, D., Spinu, V., Takahashi, K., Vaughan, D., Wilke, C., Woo, K., Yutani, H., 2019. Welcome to the Tidyverse. J. Open Source Softw. 4 (43), 1686.
Witzgall, K., Vidal, A., Schubert, D.I., Höschen, C., Schweizer, S.A., Buegger, F., Pouteau, V., Chenu, C., Mueller, C.W., 2021. Particulate organic matter as a functional soil component for persistent soil organic carbon. Nat. Commun. 12 (1) https://doi.org/10.1038/s41467-021-24192-8.
Yin, R., Eisenhauer, N., Schmidt, A., Gruss, I., Purahong, W., Siebert, J., Schädler, M., 2019. Climate change does not alter land-use effects on soil fauna communities. Appl. Soil Ecol. 140, 1–10.
Young, I.M., Crawford, J.W., 2004. Interactions and self-organization in the soil-microbe complex. Science 304, 1634–1637. https://doi.org/10.1126/science.1097394.
Zech, S., Schweizer, S.A., Bucka, F.B., Ray, N., Kögel-Knabner, I., Prechtel, A., 2022. Explicit spatial modeling at the pore scale unravels the interplay of soil organic carbon storage and structure dynamics. Glob. Chang. Biol. 28, 4589–4604. https://doi.org/10.1111/gcb.16230.
Zhou, H., Whalley, W.R., Hawkesford, M.J., Ashton, R.W., Atkinson, B., Atkinson, J.A., et al., 2020. The interaction between wheat roots and soil pores in structured field soil. J. Exp. Bot. 72, 747–756. https://doi.org/10.1093/jxb/eraa475.